Mechanism of oxygen reduction by metallocenes near liquid|liquid interfaces

T. Jane Stockmann [a], Haiqiang Deng [a], Pekka Peljo [a,b], Kyösti Kontturi [b], Marcin Opallo [c], Hubert H. Girault [a,*]

[a] Laboratoire d'Electrochimie Physique et Analytique, Ecole Polytechnique Fédérale de Lausanne (EPFL), Station 6, CH-1015 Lausanne, Switzerland
[b] Department of Chemistry, Aalto University, P.O. Box 16100, 00076 Aalto, Finland
[c] Institute of Physical Chemistry, Polish Academy of Sciences, ul. Kasprzaka 44/52, 01-224 Warszawa, Poland

ABSTRACT

The mechanism of the oxygen reduction reaction (ORR) at a liquid|liquid interface, employing ferrocene (Fc) derivatives – such as decamethylferrocene (DMFc) – as a lipophilic electron donor along with sulfuric acid as an aqueous proton source, was elucidated through comparison of experimentally obtained cyclic voltammograms (CVs) to simulated CVs generated through COMSOL Multiphysics software which employs the finite element method (FEM). The simulations incorporated a potential dependent proton transfer (i.e. ion transfer, IT) step from the water (w) to organic (o) phases along with two homogeneous reactions (C_1C_2) occurring in the organic phase – an IT-C_1C_2 mechanism. The reaction of DMFc with $H^+(o)$ to form DMFc-hydride (DMFc-H^+) was considered the first step (reaction 1), while reaction of DMFc-H^+ with oxygen to form a peroxyl radical species, HO_2, and DMFc$^+$ was deemed the second step (reaction 2). Subsequent reactions, between HO_2 and either DMFc or H^+, were considered to be fast and irreversible so that 2 was a 'proton-sink', such that further reactions were not included; in this way, the simulation was greatly simplified. The rate of 1, k_{cf}, and 2, k_{chem}, were determined to be 5×10^2 and 1×10^4 L mol^{-1} s^{-1}, respectively, for DMFc as the electron donor. Similarly, the rates of biphasic ORR for 1,1′-dimethylferrocene (DFc) and Fc were considered equivalent in terms of this reaction mechanism; therefore, their rates were determined to be 1×10^2 and 5×10^2 L mol^{-1} s^{-1} for 1 and 2, respectively. The reactive and diffusive layer thicknesses are also discussed.

© 2014 Elsevier B.V. All rights reserved.

1. Introduction

The oxygen reduction reaction (ORR) has been investigated extensively over the past 30 years owing in part to its biological significance [1,2] as well as possible applications in fuel cell technologies [3–11]. In biological systems, oxygen is an electron acceptor in the electron transport chain; this is a key step in cellular respiration that occurs as a trans-membrane process ultimately generating adenosine triphosphate (ATP), the so-called 'energy currency' of the cell, and is housed predominately in the mitochondria [1,2].

The interface between two immiscible electrolytic solutions (ITIES) provides a useful biomimetic utility for the investigation of trans-membrane processes, like ORR [12–17]. The liquid|liquid interface behaves as the junction for charge separation such that the two phases are typically composed of water (w) and an organic

solvent, such as 1,2-dichloroethane (DCE) [12–15]; indeed, this is similar to the behavior exhibited at biological membranes. The potential across the ITIES, called the Galvani potential difference, can be controlled in two ways. First, ions of intermediate solubility can be dissolved in one phase so that their partitioning across the interface generates a potential difference [18,19]. More commonly, the potential can be controlled externally through the use of a potentiostat and electrodes immersed in either phase [12–15]. In this second case, electrochemical measurements can be acquired and are analogous to those obtained through conventional solid–solution, or solid-electrolyte, interfaces. For liquid|liquid electrochemistry, the potentials in the water, ϕ_w, and organic, ϕ_o, phases can be used to control the Galvani potential difference, $\Delta_o^w \phi = \phi_w - \phi_o$, which then becomes the driving force for ion transfer (IT) [12,13].

Biphasic ORR is a key chemical process that has been studied extensively [6,16,20–25] over the past decade by groups such as Kihara et al. [26], Samec et al. [24], Opallo et al. [25], as well as our group [20,22,23,27]. These studies have typically used an

* Corresponding author. Tel.: +41 21 693 3145; fax: +41 21 693 3667.
E-mail address: hubert.girault@epfl.ch (H.H. Girault).
URL: http://www.lepa.epfl.ch/

organometallic catalyst, for example porphyrins, along with an electron donor, such as ferrocene (Fc) or decamethylferrocene (DMFc) [23,24]. As demonstrated recently using biscobalt co-facial porphyrins [23], oxygen, through a proposed mechanism studied using density functional theory (DFT), is first bound to the metal center, while acid in the aqueous phase and a Fc derivative in the organic phase provided the protons and electrons, respectively. ORR can also take place without the addition of a catalyst, *i.e.* DMFc and other Fc derivatives can perform ORR, albeit at reduced rates of reaction [21,24]; the mechanism of this reaction was again investigated using DFT calculations where it differed somewhat from the porphyrin catalyzed pathway. Therein, the first step was proton binding to the iron center to form DMFc-hydride [20]. This would subsequently react with dissolved oxygen to form a hydrogen peroxyl radical species that, through further steps, generates the reduction products H_2O_2 or water [20].

The ORR is of considerable importance at both solid-electrolyte [28–30] and liquid|liquid [6,20–26] interfaces owing to its role in possible fuel cell and energy conversion applications. The liquid|liquid interface, between water and an organic solvent, affords several advantages over conventional solid-electrolyte studies in that aqueous acids, such as HCl or H_2SO_4, can be employed while organic acids can be avoided – such as would be necessary for a homogenous organic solvent approach. Additionally, many hydrophobic organometallic catalysts are available, whilst there are very few water-soluble versions that would be required for a single-phase aqueous system. In this way, the two phases provide a convenient method for separating reagents and using existing compounds, while the liquid|liquid interface behaves as a junction for charge separation and is a facile biomimetic [12,13]. With this in mind, biphasic electrochemistry at a large ITIES (centimeter scale) was used to investigate the ORR.

Understanding the mechanism of ORR as well as the kinetics/thermodynamics of such reactions is advantageous as it allows for a modicum of prediction towards possible successful avenues of future research by highlighting significant structural, physicochemical, or reaction conditions. In this way, computational analysis in the form of DFT [21] and finite element analysis, or method (FEM) [31–34], has been used, in tandem with experimental data, to confirm or elucidate proposed reaction pathways. Herein, COMSOL Multiphysics software employing FEM was utilized, with comparison to experimental curve features found in the cyclic voltammetric (CV) experimental data, to further understand ORRs facilitated by DMFc, 1,1′-dimethylferrocene (DFc), and Fc at the w|DCE interface. In this case, it is proposed that DMFc, dissolved in the organic phase, reacts with protons pumped across the interface through three reaction steps to reduce dissolved oxygen (O_2) to hydrogen peroxide (H_2O_2).

2. Simulation

COMSOL Multiphysics version 3.5a, and similar programs utilizing FEM, have been used successfully to simulate a wide variety of processes including surface analysis through Scanning Electrochemical Microscopy [15,35], human neural response to an applied electric field for research into the treatment of Parkinson's disease [36], two-dimensional bipolar electrochemistry [37], solid oxide fuel cells [38], and IT at an ITIES [15,31–34,39,40]. Owing to the incorporation of geometry within the simulation environment, the results take on new meaning beyond those possible with simple numerical computations. Indeed, these types of simulations have been used to predict possible changes in the current–potential response of IT processes brought about by varying geometries of a micro-ITIES held at the tip of a micropipette [31,33,40].

An advantage of COMSOL software is the ability to solve multiple equations, linear or non-linear, simultaneously, such that the diffusion of species through a solution can be coupled with heterogeneous or homogeneous chemical reactions as well as IT. This aspect is of considerable interest in complex, multi-step reactions where it is difficult to differentiate between possible mechanistic pathways. As an example, Kakiuchi et al. [32] used this technique to elucidate the mechanism and kinetics/thermodynamics of interfacial complexation reactions between metal ions dissolved in an aqueous phase and ionophores placed in an ionic liquid; in that report [32], they compared experimentally obtained CVs with simulated ones. Herein, COMSOL is used to evaluate a possible ORR pathway at the w|DCE interface in a similar way, through comparison to features present in CV experimental data.

Fig. 1A illustrates a typical large (centimeter scale) four electrode liquid|liquid electrolytic cell, including a blow-up of the ITIES with the two dimensional simulation geometry marked using a red box. Fig. 1B displays the details of the simulation environment which constituted a radial cross-section of the circular ITIES including the subdomains 1 and 2 used to represent the organic (o) and water (w) phases, respectively. These subdomains are enclosed by ten external boundaries and divided by one internal boundary such that the geometry is a two-dimensional cross-section of the area surrounding the ITIES; in order to reduce computational time further it was recognized that a radial axis-of-symmetry remained, perpendicular to the interface and the simulation environment was reduced by half. A detailed description of the simulation boundary conditions have been given in the caption of Fig. 1; however, boundary 5 is significant as it was the w|o interface and was used to describe the flux of species – its boundary condition was set as 'flux'. IT at boundary 5, of the form:

$$i_w^{z_i} \rightleftharpoons i_o^{z_i} \tag{1}$$

where ion i of charge z_i transfers from w to o, was approximated using Butler–Volmer kinetics which describe the forward (k_f) and reverse (k_b) rate constants through the following, facile potential dependent equations:

$$k_f = k^0 \exp\left[-\alpha f(\Delta_o^w \phi - \Delta_o^w \phi^{0'})\right] \tag{2}$$

$$k_b = k^0 \exp\left[(1-\alpha)f(\Delta_o^w \phi - \Delta_o^w \phi^{0'})\right] \tag{3}$$

In Eqs. (2) and (3), k^0 is the standard rate constant, α is the transfer coefficient (assumed to be 0.5 unless otherwise stated), and $f_i = z_i F/RT$; such that F, R, and T are Faraday's constant, the universal gas constant, and temperature in Kelvin, respectively. $\Delta_o^w \phi$ was applied in the simulation through the use of a triangular waveform [40] implemented directly into Eqs. (2) and (3); thus, generating a potential sweep with time analogous to the scanning programs found in CV. Finally, $\Delta_o^w \phi^{0'}$ is the formal IT potential, which is a constant and property individual to each species and biphasic system.

Mass transport within each phase was handled using Fick's laws of diffusion and this is given below for the cylindrical coordinate system employed herein:

$$\frac{\partial c_{i,w}(r,z,t)}{\partial t} = D_{i,w}\left(\frac{\partial^2 c_{i,w}(r,z,t)}{\partial r^2} + \frac{1}{r}\frac{\partial c_{i,w}(r,z,t)}{\partial r} + \frac{\partial^2 c_{i,w}(r,z,t)}{\partial z^2}\right)$$
$$= D_{i,w}\nabla c_{i,w}(r,z,t) \tag{4}$$

where $D_{i,w}$ and $c_{i,w}$ are the diffusion coefficient and concentration of species i in phase w and ∇ is the gradient operator; an analogous equation can be written for species in the organic phase.

The current response with respect to charge transfer across the ITIES at boundary 5, was calculated as the integral of the flux of ions at the interface as given below:
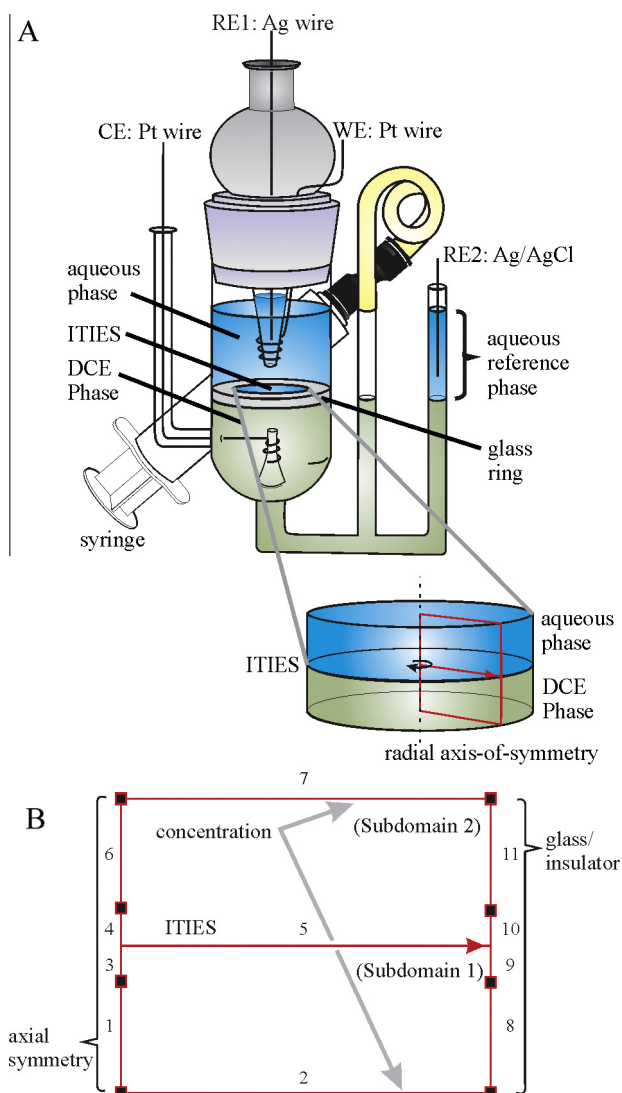
Fig. 1. A. A typical large (centimeter) four electrode, glass electrolytic cell that is open to the atmosphere (*i.e.* not air-tight) used for liquid|liquid electrochemical experiments. Also shown is a blow-up of the interface with the 2-D area representing the geometry of the simulation marked in red. B. Illustrates the 2-D radial cross-section of the large ITIES used as the simulation geometry and drawn in COMSOL Multiphysics. The geometry was composed of subdomains 1 and 2 for the organic and aqueous phases, respectively, along with 10 external and one internal boundary. The boundary condition 'axis-of-symmetry' was chosen for boundaries 1, 3, 4, and 6, as this was the center of rotation for the radial geometry, while boundaries 8, 9, 10, and 11 were designated as glass/insulator. Boundaries 2 and 7 were given the condition 'concentration' as to represent the semi-infinite (on the time scale of the simulation) concentration of species available from the bulk two phases, while boundary 5 described the w|o interface and was given the condition 'flux'. These boundary conditions have been noted within the diagram. (For interpretation of the references to colour in this figure legend, the reader is referred to the web version of this article.)

$$I = 2\pi z_i F \int \left(-D_{i,w} \nabla c_{i,w}(r,z,t) \right) r dr \tag{5}$$

Fig. S1A, of the Supplementary Information (SI), shows the CV obtained for simple IT using this system with a scan rate (v) of 0.020 V s^{-1}, a potential range from 0.000 to 0.500 V, $D_{i,w} = D_{i,o} = 1 \times 10^{-5}$ cm^2 s^{-1}, $c_{i,w}$ of 5 mmol L^{-1}, $c_{i,o}$ of 0 mmol L^{-1}, k^0 of 1 cm s^{-1}, and $\Delta_o^w \phi_i^{o'}$ equal to 0.250 V. During the forward scan, a peak-shaped wave was observed at 0.280 V and is indicative of ion transfer from w to o, while on the reverse scan, another peak-shaped wave was observed at 0.220 V and this is representative of the ions

transferring back from o to w. The half-wave potential calculated from the simulated CV was then 0.250 V, which is in excellent agreement with the defined parameters.

The shape of the simulated CV is in good agreement with the expected current–potential response at a large ITIES [13,14]; this is owing to semi-infinite linear diffusion. The peak-current is dependent on the scan rate through the Randles-Sevčik equation:

$$i_p = 0.4463 \left(\frac{F^3}{RT} \right)^{1/2} z_i^{3/2} D_{i,w}^{1/2} A c_{i,w} v^{1/2} \tag{6}$$

where A is the electrode area. Eq. (6) was used to validate the simulation mesh in that the mesh was refined until the peak-current did not change and agreed well with the calculated value; the expected value was 1.84 mA and that obtained from the simulated curve in Fig. S1A was 1.84 mA and, therefore, are in excellent agreement.

Next, the diffusion coefficient in the aqueous phase was changed to 9.3×10^{-5} cm^2 s^{-1}, to reflect the fast mass transport associated with protons moving through water, with the obtained CV displayed in Fig. S1B [41,42]. In this case, the IT half-wave potential can be predicted using a modified Nernst equation as shown below:

$$\Delta_o^w \phi_{1/2} = \Delta_o^w \phi^{o'} - \frac{RT}{z_i F} \ln \xi$$
$$\xi = \sqrt{D_{i,o}/D_{i,w}} \tag{7}$$

The value calculated using the parameters designated in the simulation along with Eq. (7) and that garnered from the simulated CV itself were both 0.279 V. The excellent agreement of these two values demonstrates the robustness of the simulation.
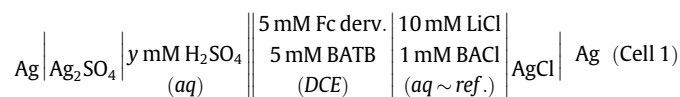
3. Experimental

3.1. Chemicals

All reagents were used as received without further purification unless otherwise mentioned. 1,2-dichloroethane (DCE, 99.9%), acetone, decamethylferrocene (DMFc, 97%), 1,1′-dimethylferrocene (DFc), ferrocene (Fc), lithium chloride, tetraethylammonium chloride (TEACl), and bis(triphenylphosphoranylidine) ammonium chloride (BACl) were purchased from Sigma–Aldrich Co. (Helsinki, Finland), while lithium tetrakis(pentafluorophenyl)borate ethyl etherate (LiTB purum) was purchased from Boulder Scientific (Longmont, CO). Sulfuric acid (0.5 M) was obtained from FF Chemicals (Haukipudas, Finland). Bis(triphenylphosphoranylidine) ammonium tetrakis(pentafluorophenyl)borate (BATB) was prepared using a metathesis reaction between LiTB and BACl in a 50%/50% (v/v) water/methanol mixture and recrystallized from acetone as published elsewhere [43]. Pt-disk microelectrodes were prepared as has been previously described [22,34].

3.2. Instrumentation

Electrochemical measurements were performed under aerobic conditions, unless otherwise stated, inside a Faraday cage using an Autolab PGSTAT100 (Ecochemie, the Netherlands) four electrode potentiostat. The working and counter electrode leads were attached to platinum wires fixed in either phase and used to monitor the current, while two reference electrodes immersed in either phase, made proximal to the ITIES through the use of Luggin capillaries incorporated in the cell design, were used to control the interfacial potential (where it is effectively described relative to the aqueous phase). Bis(triphenylphosphoranylidine) ammonium tetrakis(pentafluoro-phenyl)borate (BATB) was the organic phase supporting electrolyte and sulfuric acid was the source of protons

as well as the supporting electrolyte in the aqueous phase in the following electrochemical cell:

$$\text{Ag}\left|\text{Ag}_2\text{SO}_4\left|\begin{array}{c}y \text{ mM H}_2\text{SO}_4\\(aq)\end{array}\right|\right|\begin{array}{c}5 \text{ mM Fc derv.}\\5 \text{ mM BATB}\\(DCE)\end{array}\left|\begin{array}{c}10 \text{ mM LiCl}\\1 \text{ mM BACl}\\(aq \sim ref.)\end{array}\right|\text{AgCl}\right|\text{Ag} \quad (\text{Cell 1})$$

where the concentration of H_2SO_4 (y) was changed from 0.5 mM to 5, 50, and 500 mM, while 'Fc derv.' was either DMFc, DFc, or Fc as indicated.

3.3. Computations

All computations were carried out using COMSOL Multiphysics 3.5a on a Macintosh computer with four 2.66 GHz Intel Xeon processors, 9.8 GB of RAM, and the Ubuntu operating system; each simulation required approximately 25–30 min to complete.

4. Results and discussion

The bold curve drawn in Fig. 2 shows an experimentally obtained CV using Cell 1 with 0.5 mM H_2SO_4 in the aqueous phase under aerobic conditions, but with no Fc derivative present; essentially a 'blank' CV. The CV was swept from 0.000 V at a rate of 0.050 V s^{-1} with a potential range of approximately ±0.500 V; this range constitutes the polarizable potential window (PPW) available at the liquid|liquid interface. The rise in current at positive potentials and the decrease in current at negative potentials are caused by the transfer of the ions constituting the supporting electrolyte.

The potential scale of the blank – and all experimental CVs unless otherwise noted – have been calibrated by addition of an internal standard of known IT potential in conjunction with an extra-thermodynamic assumption known as the tetraphenylarsonium-tetraphenylborate (TATB) or Parker's assumption [44,45]. Herein, tetraethylammonium (TEA$^+$) was used as the internal standard with a standard IT potential, $\Delta_o^w\phi_{\text{TEA}^+}^o$, of 0.019 V [46].

The blank CV in Fig. 2 highlights a curve feature of interest: after the switching potential, during the reverse scan from 0.500 to −0.500 V, a return peak can be observed at 0.490 V. This corresponds to the transfer of protons back across the ITIES from o to w. An opposite intensity but analogous return peak was recorded

Fig. 2. Cyclic voltammograms (CVs) acquired using Cell 1 with 5 mM of DMFc in the DCE phase and 0.5, 5, 50, and 500 mM of H_2SO_4 in the aqueous phase such that the pH was roughly 3, 2, 1, and 0, respectively, as indicated. Instrument parameters included a scan rate of 0.050 V s^{-1}, with an initial potential of 0.000 V. The bold, black curve shows the system with no DMFc added to the DCE phase. The displayed CVs have been calibrated using the TATB assumption and TEA$^+$ as an internal standard with $\Delta_o^w\phi_{\text{TEA}^+}^o$ = 0.019 V [46].

during the final forward scan segment at −0.466 V and represents the return of sulfate, from o to w, back across the ITIES.

The significance of the H$^+$ return peak is made clear through comparison to the other CVs, overlaid in Fig. 2, acquired using Cell 1 with 0.5, 5, 50, and 500 mM of H_2SO_4 – indicated as pH 3, 2, 1, and 0, respectively – and 5 mM of DMFc dissolved in the DCE phase. It is recognized that, owing to sulfuric acids two pKa's [47] (−6.62 and 1.99 for H_2SO_4 and HSO_4^-, respectively), that the pH of the aqueous solutions will vary from these values slightly. The pH of the aqueous phase was measured using a pH meter and found to be, for example, 3.30, 2.09, and 1.55 for 0.5, 5, and 50 mM of H_2SO_4, respectively. Similar instrumental parameters as those described for the blank experiment were used to obtain these CVs and can be exemplified by the trace at pH 3.

During the reverse scan in Fig. 2 at pH 3, from 0.608 to −0.509 V, the return peak of H$^+$ transfer back across the ITIES is noticeably absent; however, cathodic and anodic IT waves have emerged at −0.333 and −0.223 V, respectively, which are indicative of DMFc$^+$ transfer [20] from o to w and back again. The approximate formal IT potential for DMFc$^+$, $\Delta_o^w\phi_{\text{DMFc}^+}^{o'}$, was calculated as an average between the four CVs from the midpoint between forward and reverse IT peaks to be −0.250 V; iR-compensation was used during signal acquisition and so this value should be treated as an estimate.
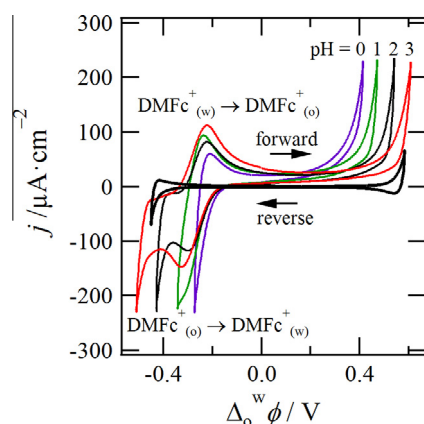
Put simply, with the addition of DMFc to the organic phase, two major changes to the CV have been noted: the appearance of DMFc$^+$ transfer and the lack of any signal for H$^+$ returning from o to w; therefore, protons must have been consumed in the organic phase in a process that generates DMFc$^+$. This is in good agreement with previous biphasic reports utilizing CV [24,48,49].

With increasing proton concentration in the aqueous phase from pH 3 to 2, 1, and 0 the limiting positive potential of the PPW decreases from 0.608 V to 0.540, 0.470, and 0.413 V, respectively, as shown in Fig. 2, with a current limit – set in the instrumental parameters – of ~230 μA cm^{-2}. This may be owing simply to the increasing supporting electrolyte concentration that has been known to limit the PPW [50]; however, it may also be the result of proton consumption in the DCE phase facilitating H$^+$ transfer and thus decreasing the amount of applied potential, or Galvani potential difference across the ITIES, necessary to elicit IT.

The CVs displayed in Fig. 2 are in good agreement with previous results by our group for the study of the ORR by DMFc [20] and 1,2-diferrocenylethane (DFcE) [22] in which DMFc$^+$ and DFcE$^+$ transfer were similarly observed. Additionally, other biphasic studies [21] have utilized UV–Vis spectroscopy to monitor the reaction progress in homogeneous DCE through the use of the DMFc$^+$ absorption peak in the visible range.
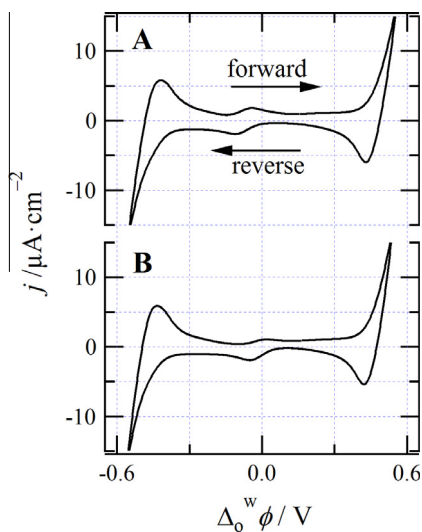
The electroactive species dimethylferrocene (DFc) and ferrocene (Fc) were also dissolved in the DCE phase and utilized in Cell 1 at 5 mM concentrations with 0.5 mM H_2SO_4 in the aqueous phase. The CVs for the DFc and Fc experiments are shown in Fig. 3A and B, respectively, where the H$^+$ return peak is still present indicating that any oxygen reduction is occurring more slowly. IT peaks for the oxidized forms of DFc and Fc were also in evidence suggesting that ORR is still taking place; however, with cathodic peak current densities of roughly −2.0 μA cm^{-2} each, it is likely, owing to the reduced reaction rate, that only a modicum of material has reacted. The formal IT potentials for DFc$^+$ and Fc$^+$ were determined to be −0.078 and −0.016 V, respectively.

In order to elucidate these processes further, COMSOL was used to generate simulated CVs through the geometry drawn in Fig. 1B, by altering the kinetic parameters. Fig. 4 illustrates the proposed reaction pathways including a potential-dependent reversible proton and DMFc$^+$ transfer steps across the ITIES along with five subsequent homogeneous reactions taking place in the organic or DCE phase.

**Fig. 3.** Cyclic voltammograms acquired using Cell 1 with 0.5 mM of H_2SO_4 in the aqueous phase as well as 5 mM of DFc (A) and Fc (B) in the organic phase. Instrument parameters were similar to those described for Fig. 2 except a scan rate of 0.020 V s^{-1} was utilized.

The first homogeneous reaction, reaction **1** from Fig. 4, is the formation of DMFc-hydride, as also given in Eq. (8):

$$DMFc_o + H_o^+ \underset{k_{cb}}{\overset{k_{cf}}{\rightleftharpoons}} DMFc\text{-}H_o^+ \quad (8)$$
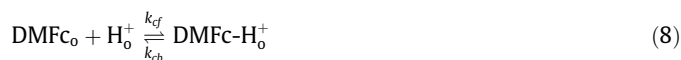
Previous DFT studies [21] suggest that a proton will first coordinate to the metal center in DMFc; however, while oxygen may coordinate [51] it is energetically unfavorable and likely a small contributor [20,21]. The latter is owing to the highly methylated cyclopentadienyl rings structurally inhibiting access to the metal center. Hydrogen is small enough to pass through, but molecular oxygen coordination requires too great a distortion, or tilting, of the cyclopentadienyl rings that is energetically prohibitive [20]. It has been shown that highly methylated cyclopentadienyl rings enhance the electron donor performance of ferrocene derivatives in ORRs [24]; in this way, the experimental results, using DFc and Fc, are in good agreement with the literature and, therefore, hydride formation was considered the logical first step in the mechanism.

The second reaction in the bulk DCE phase was the reaction of DMFc-hydride with dissolved molecular oxygen that leads to the formation of DMFc$^+$ and the hydrogen peroxyl radical species HO$_2^{\bullet}$; this is given in reaction **2** of Fig. 4 and in Eq. (9), below:

$$DMFc\text{-}H_o^+ + O_{2,o} \overset{k_{chem}}{\longrightarrow} DMFc_o^+ + HO_{2,o}^{\bullet} \quad (9)$$
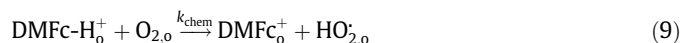
This radical species is thought to react rapidly with DMFc to form HO$_2^-$ and DMFc$^+$, shown as reaction **3** in Fig. 4. HO$_2^{\bullet}$ can either disproportionate forming oxygen and two equivalents of OH$^-$ as drawn in reaction **4** of Fig. 4, or generate hydrogen peroxide, H$_2$O$_2$, by reaction with dissolved water/protons, illustrated in reaction **5** of Fig. 4. A concerted reaction involving either two DMFc-H$^+$ molecules with diatomic oxygen was also considered possible for the generation of hydrogen peroxide, but deemed unlikely in the sense that a third order reaction would be kinetically unfavorable – or at the very least a minor contributor. Instead, the chosen simulation consisted of only reactions **1** and **2** of Fig. 4, since the subsequent reactions from HO$_2^{\bullet}$ to HO$_2^-$ and finally H$_2$O$_2$ were considered extremely fast. Regardless, all that was required of the system was an effective, so-called 'proton-sink'. Reaction **2** in Fig. 4 served this purpose by being irreversible; however, this is
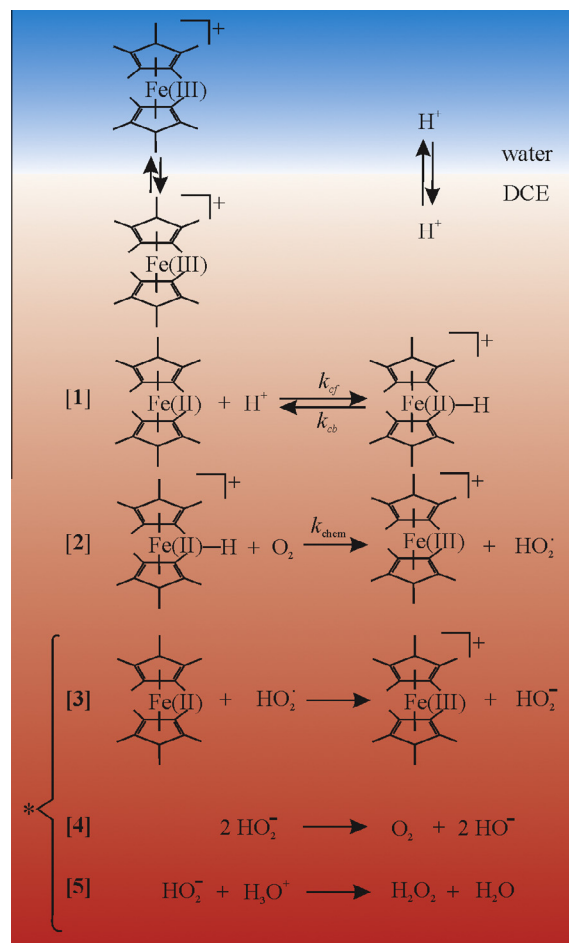
Fig. 4. Proposed mechanism for oxygen reduction at the w|DCE interface. The two potential dependent ion transfer reactions, for DMFc$^+$ and H$^+$, are shown at the top between the water (blue box) and the organic (red box) phases, while step-wise ORRs occurring in the organic phase are numbered and drawn in the red box. Reaction 1 is the DMFc-H$^+$, or hydride formation, **2** is the reaction of DMFc-H$^+$ with O$_2$ to form DMFc$^+$ and HO$_2$, **3** is the one electron oxidation of DMFc by the hydroxyl radical species, **4** is the disproportionation of HO$_2^-$ to oxygen and two equivalents of OH$^-$, and **5** is the reaction of HO$_2^-$ with an acid to form hydrogen peroxide and water. Reactions marked with an asterisk were assumed to be fast and irreversible. (For interpretation of the references to colour in this figure legend, the reader is referred to the web version of this article.)

more a reflection of the kinetics and favorability of reactions **3**–**5** then the reversibility of **2**. This had the benefit of limiting the number of dependent variables within the simulation and thus, reducing computational time. However, it should be noted that while one DMFc$^+$ molecule is generated through **1** and **2**, the second DMFc$^+$ generated in **3** was not included. If hydrogen peroxide is further reduced to water, then two more DMFc$^+$ molecules will be produced. This means that the peak current densities for DMFc$^+$ transfer can be multiplied by as much as a factor of two.
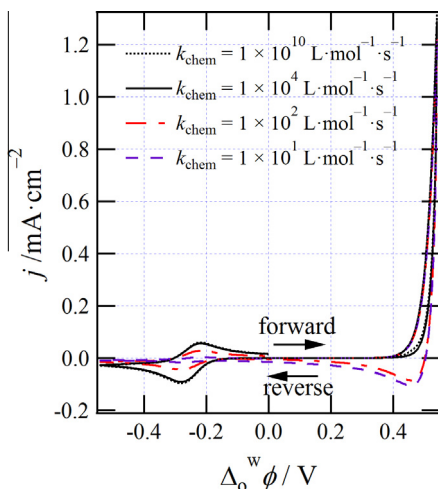
Moving forward, the simulation described in Section 2 was adapted to include the homogeneous and heterogeneous reactions outlined in Fig. 4. First, the effect of changing the rate of **2** was investigated.

Fig. 5 illustrates the simulated CVs obtained using this system, such that the simulation parameters were set to closely approximate those employed experimentally. These included a scan rate of 0.050 V s^{-1}, an initial aqueous H$^+$ concentration of 0.010 mol L^{-1}, 0.005 mol L^{-1} of DMFc in the organic phase, 0.001 mol L^{-1} of O$_2$ [52,53], and a potential range of ±0.540 V. Kinetic parameters included D_{O_2}, $D_{DMFc^+,o}$, $D_{H^+,w}$, $D_{H^+,o}$, k_{cf}, and k_{cb},

that were maintained at 2.8×10^{-5} cm^2 s^{-1} [54], 7.3×10^{-5} cm^2 s^{-1}, 9.3×10^{-5} cm^2 s^{-1} [41,42], 0.5×10^{-5} cm^2 s^{-1}, 1×10^3 L mol^{-1} s^{-1}, and 1 s^{-1}, respectively. The diffusion coefficient of DMFc$^+$ was assumed to be equal in both phases and was determined using a Pt-disk microelectrode immersed in a DCE solution of 5 mM DMFcTB (DMFc$^+$ paired with TB$^-$) with 5 mM BATB as supporting electrolyte (data not shown). The formal IT potentials, $\Delta_o^w \phi_{H^+}^{o'}$, and $\Delta_o^w \phi_{DMFc^+}^{o'}$, were set equal to 0.580 V [43] and -0.250 V, respectively. The standard rate constant, k^o, for the Butler–Volmer IT kinetics reflects the reversibility of the charge transfer reaction. The experimental reversibility of DMFc$^+$, DFc$^+$, and Fc$^+$ can be assessed through facile examination of the peak-to-peak separation (ΔE_p) between the cathodic and anodic IT waves; in this case, DMFc$^+$ ranged from roughly 0.090 to 0.104 V, while DFc$^+$ and Fc$^+$ were 0.070 and 0.061 V, respectively. Typically, for a reversible system considering an ion of charge 1+, ΔE_p should equal 0.059 V [55]. Therefore, these peak-to-peak separations indicate DMFc$^+$ and DFc$^+$ transfer to be quasi-reversible, while Fc$^+$ is essentially reversible. This trend of increasing irreversibility, DMFc$^+$ > DFc$^+$ > Fc$^+$, mirrors the trend of increasing hydrophicity of these ions and may be responsible for the increase in ΔE_p, such that ferrocene species with more methylated cyclopentadienyl rings favor the organic phase. However, while iR compensation was applied, this change may still be owing to uncompensated solution resistance. Nevertheless, for simplicity a k^o of 1 cm s^{-1} was used, which is indicative of fully reversible IT.

The rate of **2**, k_{chem} in Fig. 4, was varied from 1×10^1 L mol^{-1} s^{-1} to 1×10^2, 1×10^4, and finally 1×10^{10} L mol^{-1} s^{-1}.

When k_{chem} is equal to 1×10^1 and 1×10^2 L mol^{-1} s^{-1} reaction **2** becomes the rate-determining, or rate-limiting step. This results in large H$^+$ return peaks at ~0.455 V with magnitudes of -104 and -85 μA cm^{-2} as well as DMFc$^+$ ion transfer peaks with cathodic intensities of -15 and -44 μA cm^{-2} for the former and latter k_{chem} values, respectively. Therefore, even at low orders of magnitude for k_{chem} relative to k_{cf}, an electrochemically observable amount of DMFc$^+$ and thus, H$_2$O$_2$ is being produced. As k_{chem} increases the H$^+$ return peak decreases significantly and once it exceeds k_{cf} the curve feature is essentially absent, as can be seen with k_{chem} equal to 1×10^4 and 1×10^{10} L mol^{-1} s^{-1} in Fig. 5. Likewise, as k_{chem} increases the concentration of DMFc$^+$ generated also increases, that

in turn increases the DMFc$^+$ transfer peak intensity; the cathodic currents for both 1×10^4 and 1×10^{10} L mol^{-1} s^{-1} were observed to be -182 and -202 μA cm^{-2}, after generation of the second DMFc$^+$ is considered. These peak current densities are in fair agreement with the experimental data for DMFc, which provided average DMFc$^+$ transfer peaks of roughly -160 μA cm^{-2}. This also demonstrates that even though reaction **1** is rate determining in these later two simulations, significant increases in the rate of reaction **2** can still produce appreciable changes in the CVs.

Next, k_{cf} was altered while k_{chem} was held equal to 1×10^8 L mol^{-1} s^{-1}; the obtained, simulated CVs have been plotted in Fig. 6 for k_{cf} equal to 1×10^4, 1×10^5, and 1×10^6 L mol^{-1} s^{-1}, whereby reaction **1** is always rate determining. Owing to the fast DMFc-hydride formation, there is no observable return peak for H$^+$. The potential range was maintained at ±0.540 V in order to facilitated comparisons between the simulated and experimental CVs. An increase in the overall rate of the reactions shown in Fig. 4 generates a significant change in the current–potential profile at the edge of the PPW. For k_{cf} equal to 1×10^4 L mol^{-1} s^{-1}, this translates to an increase in the current at the edge-of-scan, I_{eos}, from ~1 mA cm^{-2} in Fig. 5 to ~1.5 mA cm^{-2} in Fig. 6.

The reaction scheme outlined in Fig. 4 can be split into an electrochemical step, the potential dependent proton transfer, followed by two chemical steps, the homogeneous reactions taking place in the organic phase; an IT-C$_1$C$_2$ mechanism. As the rate of reaction **1** increases, protons in the organic phase are quickly consumed and this results in a shift in the potential of proton transfer. This phenomena can be seen in Fig. 6 with k_{cf} equal to 1×10^5 and 1×10^6 L mol^{-1} s^{-1}, such that during the forward scan, from 0.000 to 0.540 V, a peak-shaped wave was observed, for the two rates, at 0.493 and 0.430 V, respectively. The IT-C$_1$C$_2$ mechanism is similar in some respects to interfacial complexation reactions that have been studied extensively at liquid|liquid interfaces [56–59]. The DMFc-hydride is, in essence, a metal–ligand complex and, in this way, the electrochemical mechanism described herein follows the classical interfacial complexation scheme, described by Shao et al. [60], Koryta [61], as well as recently by Molina et al. [62], often abbreviated TOC: transfer of an ion followed by organic phase complexation. Thus, the peaks observed during the forward scan for higher values of k_{cf} in Fig. 6 are the facilitated ion transfer of protons from the aqueous to organic phase; however, because k_{chem} is also high, this means that protons are consumed during the chemical step and are unavailable for return across the
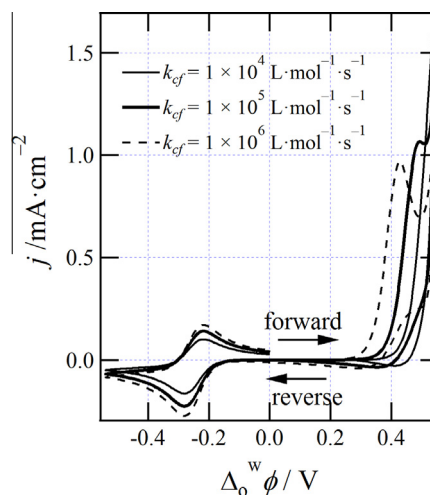

Fig. 5. Simulated cyclic voltammograms generated using the geometry shown in Fig. 1B and the mechanism illustrated in Fig. 3. The following coefficients were used: $k_{cf} = 1 \times 10^3$ L mol^{-1} s^{-1}, $k_{cb} = 1$ s^{-1}, $\Delta_o^w \phi_{H^+}^{o'} = 0.580$ V, $\Delta_o^w \phi_{DMFc^+}^{o'} = -0.250$ V, $k^0 = 1$ cm s^{-1} (for both H$^+$ and DMFc$^+$ ion transfers), $v = 0.050$ V s^{-1}, a potential range of ±0.540 V, $c_{H^+,w} = 0.010$ mol L^{-1}, $c_{DMFc,o} = 0.005$ mol L^{-1}, $c_{O_2,o} = 0.001$ mol L^{-1}, $D_{H^+,w} = 9.3 \times 10^{-5}$ cm^2 s^{-1}, $D_{H^+,o} = 0.5 \times 10^{-5}$ cm^2 s^{-1}, $D_{DMFc,o} = D_{DMFc^+,o} = D_{DMFc^+,w} = 0.7 \times 10^{-5}$ cm^2 s^{-1}, and k_{chem} as indicated.

Fig. 6. Simulated cyclic voltammograms using the same coefficients and geometry as detailed in Fig. 5, except that k_{chem} was maintained at 1×10^8 L mol^{-1} s^{-1} while k_{cf} was varied as indicated.
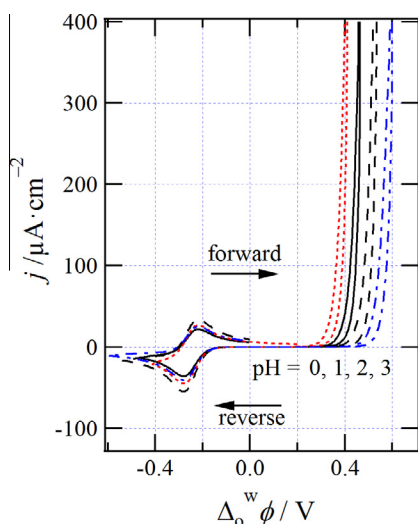
interface. This in turn generates an irreversible IT wave on the return scan.

Additionally, as k_{cf} increases the DMFc$^+$ transfer peak intensity also increases, just as in the case of k_{chem}. In Fig. 6 for k_{cf} equal to 1×10^4, 1×10^5, and 1×10^6 L mol^{-1} s^{-1} the negative peak current increases from 140 μA cm^{-2} to 226, and 272 μA cm^{-2} that becomes 280, 452, and 544 μA cm^{-2}, respectively, if the generation of a second equivalent of DMFc$^+$ is considered. This alludes to two critical findings. First, since the DMFc$^+$ transfer peak current intensity has exceeded that found experimentally, it can be concluded that the ORR taking place in the DCE phase is not limited by the diffusion of DMFc at experimental concentrations. However, the simulated case plotted in Fig. 6 is limited by the diffusion of DMFc in that the IT-C$_1$C$_2$ mechanistic peak (or essentially the FIT peak) is followed by conventional proton transfer. Secondly, this suggests that the rate of the reaction is in a range measurable by CV.

Moving forward, the simulated curves displayed in Fig. 7 were generated in order to mirror, or recreate, the experimental CVs plotted in Fig. 2. These traces were generated using the same simulation parameters as described for Fig. 5 except that a k_{chem} and k_{cf} of 1×10^4 and 5×10^2 L mol^{-1} s^{-1}, respectively, were utilized while the H$^+$ concentration was varied. As the pH of the solution decreased, the potential at the edge of scan was also decreased from 0.601 V to 0.540, 0.467, and 0.413 V for pH 3, 2, 1, and 0, respectively, in an analogy of the experimental curves displayed in Fig. 2. This is in good agreement with the IT-C$_1$C$_2$ mechanism, such that the IT of the protons, is concentration dependent [58].

However, current density at the edge of scan, I_{eos}, was found to be 466, 846, 506, and 595 μA cm^{-2} for pHs 3, 2, 1, and 0, respectively, where the experimental case for all proton concentrations was roughly 230 μA cm^{-2} throughout. I_{eos} corresponds to the amount of protons transferred across the interface such that, the magnitude of the potential range, in conjunction with the I_{eos}, becomes a curve feature to be optimized. However, this optimization cannot be performed in isolation and the two other curve features, DMFc$^+$ transfer and the proton return peak intensities, must be taken into account.

Curve matching the peak intensity of DMFc$^+$ transfer between the actual and simulated CVs is complicated by two experimental factors. First, despite purifying via sublimation the commercial DMFc, some DMFc$^+$ is present and can contribute to the signal intensity; however, this is often considered negligible. Secondly, while every attempt was made to acquire the first scan of the system during experimentation, it is often necessary to perform multiple (2 or 3) scans in order to establish the experimental potential range; this may generate a build-up of oxidized DMFc at the interface and increase the current response of its IT. Fig. S2 illustrates the result of scanning the PPW 3 times, with the traces overlaid, and demonstrates an appreciable increase in the cathodic IT peak intensity for DMFc$^+$ with values of −90, −136, and −172 μA cm^{-2} (for 2 equivalents of DMFc$^+$) for scans 1, 2, and 3, respectively, for the cathodic sweep. In this way, the peak intensity is in good agreement with that observed experimentally. The I_{eos} does not change appreciably with increasing scans and this is owning to the high effective diffusion coefficient of protons in the aqueous phase that quickly replenish the H$^+$ concentration near the interface.

A number of factors may affect the H$^+$ return peak and the I_{eos}. To explore proton transfer further a chronoamperometric (CA) potential step, from 0.000 to 0.540 V, was added to the simulation and using the same simulation parameters described for Fig. 7, with $c_{H^+,w}$ equal to 0.010 mol L^{-1}, the CA curve drawn in Fig. S3 was generated. This trace demonstrates the expected current density versus time progression, in that, as the potential is held, species steadily transfer (*i.e.* are consumed) and the response is a steady decay.

The concentration profile of protons around the interface, without DMFc present, is displayed graphically in Fig. 8 for five time intervals – 5, 10, 15, 20, and 25 s – such that $x = 0$ is the ITIES while positive and negative x, the left and right panels of Fig. 8, correspond to the aqueous and organic phase, respectively. Inset in Fig. 8 reveals the proton concentration profile on the organic phase with DMFc added along with k_{cf} and k_{chem} equal to 5×10^2 and 1×10^4 L mol^{-1} s^{-1}, respectively.

As time progresses the concentration of protons near the interface on the aqueous side decreased slightly, while the organic side observed a small increase. After 25 s – steady state conditions – protons have penetrated almost 0.40 mm into the organic phase for the system without DMFc added, whereas, for the system with DMFc, this depth is reduced to 0.06 mm. The former and latter are indicative of the diffusion (δ_d) and reaction (δ_r) layers, respectively. The latter is indicative of the rapid proton consumption through reactions **1** and **2** and may indicate that the IT-C$_1$C$_2$ mechanism is trending towards a more direct interfacial pathway; *i.e.* the proton/DMFc TOC route employed may be moving towards a transfer through interfacial complexation/decomplexation (TIC/TID)
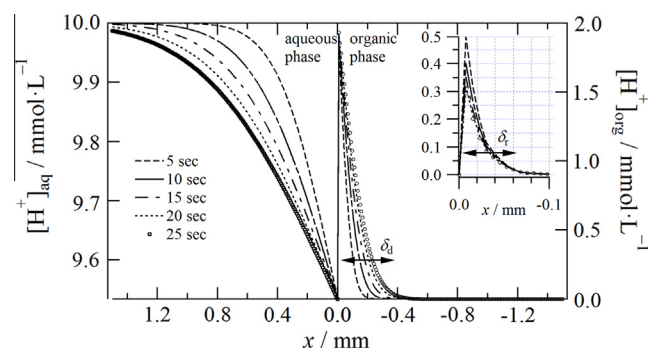

Fig. 7. Simulated cyclic voltammograms generated using the same parameters as listed for Fig. 4, save that the k_{chem} and k_{cf} were held equal to 1×10^4 and 5×10^2 L mol^{-1} s^{-1}, respectively, while $c_{H^+,w}$ was varied from 0.001 to 0.010, 0.100, and 1.000 mol L^{-1} as indicated.

Fig. 8. The proton [H$^+$] concentration profile surrounding the interface ($x = 0.0$ mm) between w (positive x) and o (negative x) during a potential step from 0.000 to 0.540 V. The following coefficients were used: $k_{cf} = 5 \times 10^2$ L mol^{-1} s^{-1}, $k_{cb} = 1$ s^{-1}, $k_{chem} = 1 \times 10^4$ L mol^{-1} s^{-1}, and $c_{DMFc,o} = 0.000$ mol L^{-1}. Inset in the right-hand panel is the [H$^+$] concentration profile of the organic phase with $c_{DMFc,o} = 0.005$ mol L^{-1}. The diffusion (δ_d) and reaction (δ_r) layer thickness have been indicated with double arrows for the organic side.

pathway. For convenience, the ITIES utilized here is an infinitely thin compact layer; however, the interface has been shown to most likely resemble a mixed solvent layer [12,13,19] so that the system is changing from TOC to TIC/TID, and the reduction in the size of δ_r, may indicate a move towards this mixed solvent layer model. The criteria describing the trend from a IT-C_1C_2 mechanism (effectively TOC or EC mechanism) has been elucidated through rigorous treatment by Molina et al. [62], in which they differentiate between three reaction conditions: a kinetic steady state, diffusive-kinetic steady state, and a total equilibrium condition.

Additionally, since FEM is a computational treatment of chemical species which views them as concentration in an abstract sense, such that molecules do not have size or dimension, the number of surface active sites [63,64] at the ITIES is effectively infinite in a TIC/TID mechanism. This may be true at higher pH, however, as the proton concentration increases the number of available DMFc molecules may diminish limiting these 'effective' active sites. However, this is likely a minor contributor to the disparity in the I_{eos} between the experimental and simulated results.

Another explanation for the deviation in the I_{eos} is the use of $\Delta_o^w\phi_{H^+}^{o'}$ equal to 0.580 V as previously determined by our group [43]. In that article [43], the formal IT potential of protons at the w|DCE interface was determined using a microhole apparatus with minimal supporting electrolyte in the organic phase and only the analyte in the aqueous phase; the method also utilized a curve fitting algorithm – applied directly to the CVs – adapted from theory developed by Oldham [65] and Wilke [66]. While minimal supporting electrolyte was used in the organic phase [43], it has been recently shown, by Mirkin et al. [67], that even small amounts of supporting electrolyte can assist or facilitate the transfer of highly hydrophilic ions across the ITIES; essentially behaving as a ligand or complexing agent. It is also well known that increasing either the ligand or ion concentration will reduce the amount of applied potential necessary to induce FIT [58,68,69] as is seen when moving from the microhole experiment [43] – performed to obtain the formal IT potential value – to the present case; therefore, a higher $\Delta_o^w\phi_{H^+}^{o'}$ may be indicated. However, since k_{cf} and k_{chem} have a marked influence on the onset potential for proton transfer making their determination – as well as that of $\Delta_o^w\phi_{H^+}^{o'}$ – exceedingly complex and, therefore, beyond the scope of the present communication.

In order to verify the final k_{cf} value of 5×10^2 L mol^{-1} s^{-1}, two facile experiments were conducted. In the first, a blank CV was obtained using Cell 1 with 5 mM H$_2$SO$_4$ ($y = 5$) and no DMFc added in the DCE phase – the black, dashed trace in Fig. 9. Next, the cell was de-aerated and transferred to the glovebox (no oxygen present) where 5 mM of DMFc was added to the organic phase – black, dotted trace in Fig. 9. Simulated CVs were generated using the same conditions and were plotted in Fig. 9 as well, such that c_{O_2} and $c_{DMFc,o}$ were set equal to 1.3 and 0 mM or 0 and 5 mM for the thick, blue and thin, red traces, respectively. All other conditions were the same as that described for Fig. 8. The shift in onset potential for H$^+$ transfer is in good agreement between the two experimental and simulated CVs for the blank (no DMFc present), aerated (oxygen present) system and the 5 mM DMFc, anaerobic system. These two experiments provide evidence for the strength of the DMFc-hydride formation effectively in the absence of any known homogeneous reactions – aside from the hydrogen evolution reaction that may be a minor contributor in this case [70,71]. The aerobic results are in good agreement with the low value of k_{cf}, such that, with DMFc present the H$^+$ return peak persists; therefore, the DMFc-hydride formation should be reversible and also weakly coordinating.

Next, the formal IT potential for DMFc$^+$ in the simulation can be altered to reflect that of DFc$^+$ and Fc$^+$, with these CVs shown in Fig. S2A and B of the SI, such that $\Delta_o^w\phi_{DFc^+}^{o'}$ and $\Delta_o^w\phi_{Fc^+}^{o'}$ equal to
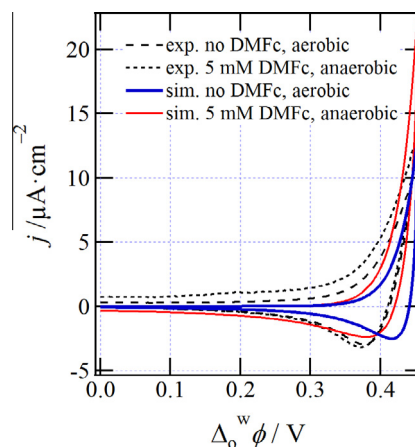
Fig. 9. Experimental cyclic voltammograms (CVs) obtained using Cell 1 with 5 mM of H$_2$SO$_4$ in the aqueous phase with no DMFc under aerobic conditions (dashed curve) or 5 mM of DMFc in the DCE phase under anaerobic conditions (dotted curve). Two simulated CVs with c_{O_2} and $c_{DMFc,o}$ equal to 1.3 and 0 mM (thick, blue curve) as well as c_{O_2} and $c_{DMFc,o}$ equal to 0 and 5 mM (thin, red curve), respectively. (For interpretation of the references to colour in this figure legend, the reader is referred to the web version of this article.)

−0.078 and −0.016 V, respectively, were utilized. For these CVs the focus was to replicate the ratio of the H$^+$ return peak to the DFc$^+$/Fc$^+$ cathodic peak intensity; i_{rp}/i_{cp}. For both species i_{rp} was approximately −6 μA cm^{-2} while i_{cp} equalled roughly −2 μA cm^{-2}, thus generating an i_{rp}/i_{cp} ratio of 3 with an I_{eos} of ∼15 μA cm^{-2}. Rates for reactions **1** and **2**, k_{cf} and k_{chem}, were set equal to 1×10^2 and 5×10^2 L mol^{-1} s^{-1}, respectively, generating i_{rp}/i_{cp} of 3 with a I_{eos} of ∼40 μA cm^{-2}. In this way, the experimental CVs plotted in Fig. S4A and B are in fair agreement with the experimental ones displayed in Fig. 3.

For all three Fc derivatives the rate determining step was reaction **1** and is in good agreement with the result recently published by Trojánek et al. [24], in which a Fc derivative with six methyl substituents on the cyclopentadienyl rings was found to have a non-catalyzed rate of 4.7×10^3 L mol^{-1} s^{-1}.

A list of the simulation parameters can be found in Table S1, including the diffusion coefficients, initial concentrations of each species in either phase, standard/formal IT potentials with calculated partition coefficients, as well as the values of k_{cf} and k_{chem} determined for each of the reducing agents. The partition coefficient, shown in Table S1, is related to potential through the following [72],

$$\ln P_i = \ln \frac{c_{i,o}}{c_{i,w}} = \ln P_i^{o'} + \frac{z_iF}{RT}\Delta_o^w\phi$$
$$\text{where, } \ln P_i^{o'} = -\frac{z_iF}{RT}\Delta_o^w\phi_i^{o'} \tag{10}$$

While ferrocenium demonstrates a moderate Gibbs energy of transfer, where $\Delta G_{tr,Fc^+}^{w\to o} = z_iF\Delta_o^w\phi_{Fc^+}^{o'}$ such that −1.5 kJ mol^{-1} for Fc$^+$ is obtained. The Gibbs energy of transfer for the neutral Fc species has been determined to be −24.5 kJ mol^{-1} [73]; from which the standard partition coefficient of Fc can be calculated through equation 10 to be 1.8×10^4. It can be concluded based on this value that a negligible concentration of Fc would transfer to the aqueous phase at equilibrium on the experimental time scale. The open circuit potential of the system was calculated, as described recently [74], using the initial experimental concentrations and found to be 0.060 V. While protons are too hydrophilic to transfer, if the solution is left for a long enough period of time, then Fc may partition to the aqueous phase, as shown recently by Opallo et al. [25], and subsequently react; however, this was found to be minor. Therefore, the IT-C_1C_2 mechanism involving strictly homogeneous organic phase ORR, as shown in Fig. 4, is reasonable on the time

scale of the CV experiment. In this way, these reactions are only induced when protons are transferred to the organic phase through an external, applied potential. To the best of our knowledge there is no published data for the partition of neutral DMFc or DFc at a w|DCE interface; however, it is reasonable to assume that these species are more hydrophobic than neutral Fc and would follow a similar mechanism of ORR – that being restricted, predominantly, to the organic phase. However a small positive offset current density was observed in Fig. 2 after addition of DMFc to the organic phase. This may suggest that DMFc does partition to the aqueous phase, reacts forming DMFc$^+$, which is in turn responsible for the offset as has previously been proposed [75]. This reaction would then serve as a driving force to 'pump' further DMFc across the ITIES. Nevertheless, the incorporation of both an aqueous and organic phase ORR mechanism was deemed too complex at present and may be the subject of a future submission.

Not included in the mechanism illustrated in Fig. 4 is the transfer of DMFc-H$^+$; however, based on the rates elucidated herein, this species should be short-lived. The rate determining step is the hydride formation and afterwards DMFc-H$^+$ is rapidly consumed – *i.e.* does not persist long enough for its IT to be consequential. Additionally, during the CV experiment the majority of protons are consumed, and thus the largest presence of DMFc-H$^+$, occurs while the interfacial Galvani potential difference is positive; therefore, any DMFc-H$^+$ would be maintained in the organic phase both due to the ITIES polarization and its hydrophobicity – which is likely similar to DMFc$^+$.

Additionally, varying scan rates of 0.010–0.100 V s^{-1} were performed both experimentally and using the simulation; the only appreciable change was an increase in the DMFc$^+$ transfer peak, as expected from the Randles-Sevčik equation, with no significant change to the H$^+$ return peak.

5. Conclusions

The ORR was explored using facile electrochemistry at a biphasic interface between water and DCE, under aerobic conditions, using DMFc, DFc, and Fc, dissolved in the organic phase, as electron donors and sulfuric acid in the aqueous phase as a proton source. Two prominent curve features within the CV were noted: the absence of a return peak current for H$^+$ at the edge of the PPW along with the emergence of an IT peak towards negative potentials that was later assigned to DMFc$^+$ transfer. It was thereby concluded that protons were being consumed in the organic phase in a reaction oxidizing DMFc. This is in good agreement with previous reports [6,20,22–25,48,49,53].

With this evidence, a mechanism was proposed and tested using a two-dimensional FEM simulation, whereby oxygen was reduced by first proton transfer to the organic phase, followed by formation of a DMFc-hydride, which would then react with dissolved oxygen to generate a peroxyl radical species, HO$_2$. It was also proposed that this radical would react quickly, with either DMFc-H$^+$ or H$_2$O and a proton, to form hydrogen peroxide completing the reduction of oxygen. In this way, potential dependent proton transfer comprised the electrochemical (*i.e.* IT) step, while the two homogeneous reactions, hydride formation and oxygen reduction, constituted the chemical step in a reaction pathway reminiscent of classical EC-mechanisms. No further reactions were included as the formation of H$_2$O$_2$ was thought to be fast and irreversible, such that the HO$_2$ step was considered a 'hydrogen-sink' for the purposes of the simulation.

Through comparison of the simulated and experimental CVs several critical insights were garnered. First, the rate of the reaction is measurable by CV and is likely between 1 and 5×10^2 L mol^{-1} s^{-1} for all three Fc derivatives and is the rate-determining

step, based on the height of the DMFc$^+$/DFc$^+$/Fc$^+$ cathodic transfer peak along with the current at the edge of scan, I_{eos}, profile. The rate of the homogeneous reaction was similarly discerned and found to be 1×10^4 L mol^{-1} s^{-1} for DMFc, but only 5×10^2 L mol^{-1} s^{-1} for DFc/Fc. Second, biphasic ORR is not dependent on the diffusion of DMFc in the organic phase. Most importantly, the simulated CVs demonstrate the feasibility of the proposed mechanism through their comparison to experimental curve features.

Conflict of interest

The authors certify no conflict to interest.

Appendix A. Supplementary material

Supplementary data associated with this article can be found, in the online version, at http://dx.doi.org/10.1016/j.jelechem.2014.07.001.

References

[1] S. O'Sullivan, D.W.M. Arrigan, Anal. Chem. 85 (2012) 1389–1394.
[2] M. Wikström, BBA – Bioenergetics 1817 (2012) 468–475.
[3] T. Yasuda, M. Watanabe, MRS Bull. 38 (2013) 560–566.
[4] J.M. Pringle, Phys. Chem. Phys. 15 (2013) 1339–1351.
[5] X. Wang, R.K. Ahluwalia, A.J. Steinbach, J. Electrochem. Soc. 160 (2013) F251–F261.
[6] P. Peljo, T. Rauhala, L. Murtomäki, T. Kallio, K. Kontturi, Int. J. Hydrogen Energy 36 (2011) 10033–10043.
[7] K. Otsuka, I. Yamanaka, Electrochim. Acta 35 (1990) 319–322.
[8] I. Yamanaka, T. Onizawa, S. Takenaka, K. Otsuka, Angew. Chem. Int. Ed. 42 (2003) 3653–3655.
[9] I. Yamanaka, T. Murayama, Angew. Chem. Int. Ed. 47 (2008) 1900–1902.
[10] A. Khan, X. Lu, L. Aldous, C. Zhao, J. Phys. Chem. C (2013), http://dx.doi.org/10.1021/jp405759j.
[11] S. Fukuzumi, H. Kotani, H.R. Lucas, K. Doi, T. Suenobu, R.L. Peterson, K.D. Karlin, J. Am. Chem. Soc. 132 (2010) 6874–6875.
[12] Z. Samec, J. Langmaier, T. Kakiuchi, Pure Appl. Chem. 81 (2009) 1473–1488.
[13] H. Girault, Electrochemistry at liquid–liquid interfaces, in: A.J. Bard, C.G. Zoski (Eds.), Electroanalytical Chemistry, CRC Press, 2010, pp. 1–104.
[14] S. Liu, Q. Li, Y. Shao, Chem. Soc. Rev. 40 (2011) 2236–2253.
[15] Y. Wang, K. Kececi, J. Velmurugan, M.V. Mirkin, Chem. Sci. 4 (2013) 3606–3616.
[16] M.D. Scanlon, ChemCatChem 5 (2013) 1696–1697.
[17] M.A. Méndez, R. Partovi-Nia, I. Hatay, B. Su, P.Y. Ge, A. Olaya, N. Younan, M. Hojeij, H.H. Girault, Phys. Chem. Chem. Phys. 12 (2010) 15163–15171.
[18] P. Ge, A.J. Olaya, M.D. Scanlon, I. Hatay Patir, H. Vrubel, H.H. Girault, ChemPhysChem 14 (2013) 2308–2316.
[19] P. Peljo, H.H. Girault, Liquid/Liquid Interfaces, Electrochemistry at, Encyclopedia of Analytical Chemistry, John Wiley & Sons Ltd., 2012.
[20] B. Su, R.P. Nia, F. Li, M. Hojeij, M. Prudent, C. Corminboeuf, Z. Samec, H.H. Girault, Angew. Chem. Int. Ed. 47 (2008) 4675–4678.
[21] B. Su, I. Hatay, P.Y. Ge, M. Mendez, C. Corminboeuf, Z. Samec, M. Ersoz, H.H. Girault, Chem. Commun. 46 (2010) 2918–2919.
[22] H. Deng, P. Peljo, F. Cortés-Salazar, P. Ge, K. Kontturi, H.H. Girault, J. Electroanal. Chem. 681 (2012) 16–23.
[23] P. Peljo, L. Murtomäki, T. Kallio, H.-J. Xu, M. Meyer, C.P. Gros, J.-M. Barbe, H.H. Girault, K. Laasonen, K. Kontturi, J. Am. Chem. Soc. 134 (2012) 5974–5984.
[24] A. Trojánek, J. Langmaier, Z. Samec, Electrochim. Acta 82 (2012) 457–462.
[25] J. Jedraszko, W. Nogala, W. Adamiak, E. Rozniecka, I. Lubarska-Radziejewska, H.H. Girault, M. Opallo, J. Phys. Chem. C 117 (2013) 20681–20688.
[26] H. Ohde, K. Maeda, Y. Yoshida, S. Kihara, J. Electroanal. Chem. 483 (2000) 108–116.
[27] H. Deng, P. Peljo, T.J. Stockmann, L. Qiao, T. Vainikka, K. Kontturi, M. Opallo, H.H. Girault, Chem. Commun. 50 (2014) 5554–5557.

[28] S.H. Park, C.H. Choi, J.K. Koh, C. Pak, S.-A. Jin, S.I. Woo, ACS Comb. Sci. 15 (2013) 572–579.
[29] N.N. Kariuki, W.J. Khudhayer, T. Karabacak, D.J. Myers, ACS Catalysis 3 (2013) 3123–3132.
[30] M.C.S. Escaño, H. Kasai, J. Power Sources 247 (2014) 562–571.
[31] N. Nishi, S. Imakura, T. Kakiuchi, J. Electroanal. Chem. 621 (2008) 297–303.
[32] N. Nishi, H. Murakami, S. Imakura, T. Kakiuchi, Anal. Chem. 78 (2006) 5805–5812.
[33] T.J. Stockmann, Z. Ding, J. Electroanal. Chem. 649 (2010) 23–31.
[34] T.J. Stockmann, Z. Ding, J. Phys. Chem. B 116 (2012) 12826–12834.
[35] D. Momotenko, L. Qiao, F. Cortés-Salazar, A. Lesch, G. Wittstock, H.H. Girault, Anal. Chem. 84 (2012) 6630–6637.
[36] A. Chaturvedi, T.J. Foutz, C.C. McIntyre, Brain Stimul. 5 (2012) 369–377.
[37] S.E. Fosdick, J.A. Crooks, B.-Y. Chang, R.M. Crooks, J. Am. Chem. Soc. 132 (2010) 9226–9227.
[38] M.A. Khaleel, Z. Lin, P. Singh, W. Surdoval, D. Collin, J. Power Sources 130 (2004) 136–148.
[39] J. Josserand, J. Morandini, H.J. Lee, R. Ferrigno, H.H. Girault, J. Electroanal. Chem. 468 (1999) 42–52.
[40] P.J. Rodgers, S. Amemiya, Anal. Chem. 79 (2007) 9276–9285.
[41] T.S. Light, S. Licht, A.C. Bevilacqua, K.R. Morash, Electrochem. Solid-State Lett. 8 (2005) E16–E19.
[42] S.H. Lee, J.C. Rasaiah, J. Chem. Phys. 135 (2011). 124505/1–124505/10.
[43] A.J. Olaya, M.A. Méndez, F. Cortes-Salazar, H.H. Girault, J. Electroanal. Chem. 644 (2010) 60–66.
[44] A.J. Parker, Electrochim. Acta 21 (1976) 671–679.
[45] K. Zhurov, E.J.F. Dickinson, R.G. Compton, J. Phys. Chem. B 115 (2011) 6909–6921.
[46] T. Wandlowski, V. Mareček, Z. Samec, Electrochim. Acta 35 (1990) 1173–1175.
[47] W.M. Haynes, Dissociation Constants of Inorganic Acids/Bases, CRC Handbook of Chemistry and Physics, CRC Press/Taylor, Boca Raton, FL, 2013, pp. 5.92.
[48] A. Trojánek, V. Mareček, H. Jänchenová, Z. Samec, Electrochem. Commun. 9 (2007) 2185–2190.
[49] A. Trojánek, J. Langmaier, B. Su, H.H. Girault, Z. Samec, Electrochem. Commun. 11 (2009) 1940–1943.
[50] J. Langmaier, Z. Samec, Anal. Chem. 81 (2009) 6382–6389.
[51] V.M. Fomin, Russ. J. Gen. Chem. 77 (2007) 954–960.
[52] P. Luehring, A. Schumpe, J. Chem. Eng. Data 34 (1989) 250–252.
[53] A. Trojánek, J. Langmaier, Z. Samec, Electrochem. Commun. 8 (2006) 475–481.
[54] A. Schumpe, P. Luehring, J. Chem. Eng. Data 35 (1990) 24–25.
[55] A.J. Bard, L.R. Faulkner, Electrochemical methods: fundamentals and applications, second ed., John Wiley, New York, 2001.
[56] T.J. Stockmann, A.-M. Montgomery, Z. Ding, Anal. Chem. 84 (2012) 6143–6149.
[57] Y. Qiao, B. Zhang, X. Zhu, T. Ji, B. Li, Q. Li, E. Chen, Y. Shao, Electroanalysis 24 (2013) 1080–1084.
[58] F. Reymond, G. Lagger, P.-A. Carrupt, H.H. Girault, J. Electroanal. Chem. 451 (1998) 59–76.
[59] U. Nestor, H. Wen, G. Girma, Z. Mei, W. Fei, Y. Yang, C. Zhang, D. Zhan, Chem. Commun. 50 (2014) 1015–1017.
[60] Y. Shao, M.D. Osborne, H.H. Girault, J. Electroanal. Chem. Interfacial Electrochem. 318 (1991) 101–109.
[61] J. Koryta, Electrochim. Acta 24 (1979) 293–300.
[62] Á. Molina, E. Torralba, C. Serna, J.A. Ortuño, J. Phys. Chem. A 116 (2012) 6452–6464.
[63] J.M. Savéant, J. Electroanal. Chem. Interfacial Electrochem. 112 (1980) 175–188.
[64] C. Amatore, F. M'Halla, J.M. Savéant, J. Electroanal. Chem. Interfacial Electrochem. 123 (1981) 219–229.
[65] K.B. Oldham, J. Electroanal. Chem. 250 (1988) 1–21.
[66] S. Wilke, J. Electroanal. Chem. 504 (2001) 184–194.
[67] P. Sun, F.O. Laforge, M.V. Mirkin, J. Am. Chem. Soc. 127 (2005) 8596–8597.
[68] T. Kakiuchi, M. Senda, J. Electroanal. Chem. 300 (1991) 431–445.
[69] Z. Samec, D. Homolka, V. Mareček, J. Electroanal. Chem. Interfacial Electrochem. 135 (1982) 265–283.
[70] I. Hatay, B. Siu, F. Li, R. Partovi-Nia, H. Vrubel, X.L. Hu, M. Ersoz, H.H. Girault, Angew. Chem. Int. Ed. 48 (2009) 5139–5142.
[71] M.D. Scanlon, X. Bian, H. Vrubel, V. Amstutz, K. Schenk, X. Hu, B. Liu, H.H. Girault, Phys. Chem. Chem. Phys. 15 (2013) 2847–2857.
[72] H. Girault, Analytical and Physical Electrochemistry, first ed., EPFL Press, Lausanne, CH, 2004.
[73] D.J. Fermin, R. Lahtinen, Dynamic aspects of heterogeneous electron-transfer reactions at liquid–liquid interfaces, in: A.G. Volkov (Ed.), Liquid Interfaces In Chemical, Biological And Pharmaceutical Applications, Marcel Dekker Inc., 2001.
[74] Y. Li, S. Wu, B. Su, Chem. Eur. J. 18 (2012) 7372–7376.
[75] B. Su, I. Hatay, F. Li, R. Partovi-Nia, M.A. Méndez, Z. Samec, M. Ersoz, H.H. Girault, J. Electroanal. Chem. 639 (2010) 102–108.